

Ripples and charge puddles in screened graphene

S. C. Martin, B. Sacépé, S. Samaddar, A. Kimouche,

J. Coraux, H. Courtois, and C. B. Winkelmann*

Institut Néel, CNRS, Université Joseph Fourier and Grenoble INP,

BP166, 38042 Grenoble cedex 9, France.

(Dated: June 20, 2022)

Abstract

At vanishing charge carrier density, graphene on a dielectric substrate exhibits spatial doping inhomogeneities forming electron-hole puddles [1]. Understanding and controlling the latter is of crucial importance for unraveling many of graphene's fundamental properties at the Dirac point, where the linear valence and conduction bands meet. Charged impurities trapped in the dielectric substrate [1-3] as well as the local graphene curvature [4-7] have been pointed to as the puddles' origin. Here we show by scanning tunneling microscopy/spectroscopy the coexistence and correlation of charge puddles and topographic ripples in graphene decoupled from a metallic Ir substrate. The perfect screening of charged impurities by the metallic substrate reveals charge puddles directly induced by the local graphene-substrate distance and the ensuing charge transfer. Furthermore, the analysis of Dirac fermion interferences shows that electron-electron interactions are also strongly screened. Our findings therefore demonstrate that graphene on Ir provides a new platform to study the non-interacting limit for massless Dirac electrons in graphene.

The study of factors liable to cause electron-hole puddles in graphene has so far relied on graphene sheets isolated by mechanical exfoliation of graphite on dielectric substrates such as SiO₂. Conflicting conclusions were drawn on the basis of different studies, some identifying exclusively charged impurities between graphene and SiO₂ as sources of the puddles [2, 3], others invoking in addition the mixing of the π and σ orbitals due to local curvature [4]. Recent theoretical works suggest that puddles might be related in a non-trivial way to the rippling of graphene [5]. In this context, the strong disorder observed in graphene on SiO₂ [8] and the limited knowledge about the graphene/SiO₂ interface calls for the use of other substrates. More generally, experiments based on different dielectric environments, that is, different strengths of charged impurities' screening have been performed. They however showed no significant influence of the dielectric constant on the electronic properties, thereby questioning the role of charged impurities for the puddle formation [9–11].

Metal supports are expected to fully screen charged impurities and thus are ideally suited for elucidating the role of other mechanisms in the puddles formation. Periodic ripples, arising from the lattice parameter mismatch between graphene and most transition metal surfaces, were for instance related to the puddles [12] in graphene on Ru(0001). It however turned out that charge carriers in this system do not exhibit Dirac fermion-like properties, due to a strong hybridization between the $4d$ Ru and p_z C orbitals [13, 14]. Even in less strongly coupled systems, interaction between graphene's conduction/valence bands with surface states of the metal [15, 16] cannot be excluded. A linear dispersion relation in the electronic band structure at the Brillouin zone corners was recovered in graphene on Ru(0001) intercalated with an atomic layer of oxygen below the graphene [17]. This layer unfortunately suppresses the graphene ripples, which prevents from addressing the possible relationship between puddles and topography.

We have performed low temperature scanning tunneling microscopy and spectroscopy (STM/STS) on graphene prepared by chemical vapor deposition on epitaxial Ir(111) under ultra-high vacuum (UHV). Exposure to air can decouple the graphene from its metallic support, transforming the moiré pattern into a disordered topographic landscape (see Supplementary Information). This system thereby offers a unique configuration to study the impact of ripples on the electronic properties of screened graphene.

We begin with a close look at the topography of graphene on a plain Ir atomic terrace. We observe a disordered topographic landscape with a typical rms roughness $\sigma_z \approx 100$ pm

(Fig. 1a), which is comparable to the corrugation of graphene on SiO₂. While the usual moiré pattern is absent, atomic resolution is routinely achieved (Fig. 1a), demonstrating the quality of the surface.

The electronic density of states can then be accessed by the measurement of the local tunneling conductance $G(V) = dI/dV$. The tunnel spectra display a V-shape (Fig. 1b), characteristic of the density of states of graphene and similar to data typically observed by STS on exfoliated graphene on SiO₂ [20, 21]. The voltage at the conductance minimum has been identified as the Dirac point (also called the charge neutrality point) at energy $E_D = eV_{min}$ in previous works [3]. The value of E_D reflects the strength of the local graphene doping [3, 4, 20], which is *p*-type here. A dip of width of about 20 meV is also present around zero bias, which is frequently reported in STS studies on graphene [20–22] and will not be discussed in this work.

We have measured a series of high-resolution conductance maps at low temperature. At each position \mathbf{r} of a tunnel conductance map, the Dirac point energy E_D is extracted using a parabolic fit around the minimum of G . The spatially averaged doping $E_D^0 = 340$ meV is larger than inferred from ARPES studies in UHV, which reported E_D at 100 meV for graphene on Ir(111) [15]. Maps such as shown in Fig. 2a picture the spatial inhomogeneities of E_D around its mean value, forming a smooth landscape of charge puddles, of about 9 nm size, see Supp. Info. for details. From $E_D^2 = (\hbar v_F)^2 \pi n$ [2], where \hbar and v_F are the reduced Planck constant and the Fermi velocity respectively, we extract the distribution of the charge carrier density n (Fig. 2b), assuming the theoretically expected value of $v_F^0 = 1.0 \times 10^6$ m/s. Notably, the standard deviation $\sigma_n \approx 9 \times 10^{11}$ cm⁻² is of the same order than that reported in graphene exfoliated on SiO₂ ($\approx 4 \times 10^{11}$ cm⁻²) [3, 23], while significantly larger than that of graphene on a boron nitride substrate ($\approx 2.5 \times 10^9$ cm⁻²) [24]. In the following, we determine the value of v_F to be 0.89×10^6 m/s in our system, which leads to refining $\sigma_n = 1.1 \times 10^{12}$ cm⁻².

We now focus on the comparison between the Dirac point distribution and the topography. Since only topographic variations at length scales similar or larger than the typical puddle size can correlate with the charge inhomogeneities, we filter out the topographic maps from structures of dimensions below half the mean puddle size. Figure 2a shows the superposition of an $E_D(\mathbf{r})$ map (color scale) along with the long wavelength-pass filtered topography $z(\mathbf{r})$ recorded at the same position (3D profile). A very high degree of correlation between doping

and topography is readily seen. We have quantified this by calculating the normalized cross-correlation function $\chi(\mathbf{r}) = \sum_i E_D(\mathbf{r}_i - \mathbf{r}) \times z(\mathbf{r}) / (\sigma_{E_D} \times \sigma_z)$ of the two data sets. The local cross-correlations $\chi(0)$ between $E_D(\mathbf{r})$ and $z(\mathbf{r})$ are in excess of 60 % in large area maps (Fig. 2c). These correlations are independent on the region chosen, but are enhanced in maps with dimensions much larger than the typical puddle size.

When correlating spectroscopic maps with topography, one has to recall that in constant-current STM mode a local DOS variation will lead to a change in the tip-sample distance z . This can misleadingly induce phantom topographic features. Because the tunnel current dependence is exponential on z while only linear on DOS variations, this contribution is however modest. We have carefully quantified it to be about 6 pm, that is, more than one order of magnitude smaller than the effects described here, see Supp. Info. for details.

With the above analysis, we arrive to the main result of this Letter: disordered graphene on a metallic substrate displays a strong local correlation between local doping and topography. It is important to note that the sign of the local cross correlations $\chi(0)$ is positive, that is, the p -doping character increases with increasing topographic height. Intuitively, one expects an infinite graphene sheet above an iridium plane to be p -doped at large distances, according to the difference in work functions of both materials. As both surfaces come closer, calculations show that the finite electronic wave function overlap leads to a cross-over towards n -type charge transfer [26]. There is thus a wide range of graphene-metal distances z at which $\partial E_D / \partial z > 0$, which is here reflected by the sign of $\chi(0)$. A contribution of curvature effects [5] could also be anticipated. In the present system, the theoretically expected contribution of this effect is however nearly two orders of magnitude below the observed amplitude of the doping disorder [25].

In order to obtain a more microscopic understanding of the role of the local electrostatic environment as electron scattering centers, we have tracked the wave vector \mathbf{k} distribution of interference patterns in the Fourier transforms of DOS maps. The evolution of the dominant \mathbf{k} , relative to the Brillouin zone corner as a function of the energy level of each map then reflects the dispersion relation of the scattered electrons. In graphene, both the large k intervalley and the small k intravalley scatterings have been observed by this technique [27]. For intravalley scattering, the wave vector transfer \mathbf{q} links two points of the circle resulting from the intersection of a given Dirac cone and a constant energy plane. A particular characteristic of graphene is the suppression of low-energy backscattering [28]. One therefore

expects a continuous distribution of q between 0 and $2k_F$ for intravalley scattering, seen as a disk in reciprocal space.

In our data, we observe the DOS maps at energies far from E_D^0 to display clearly resolved structures at length scales smaller than the typical puddle size (Figs. 3a–f). Further, the size of the observed features decreases with increasing $|E - E_D^0|$. The maps' Fourier transform maps display a disk-like structure (Fig. 3g, see also Supp. Info.) from which we extract $k = q_{max}/2$ at each energy (Fig. 3h, see also Methods). The linear behavior of $k(E - E_D^0)$ evidences the scattering mechanism at work as intravalley. It is actually notable that this can be observed in graphene on a metallic substrate at all.

A fit by the linear dispersion relation of graphene $E = E_D^0 \pm \hbar v_F k$ (Fig. 3h) yields $v_F = 0.89 \pm 0.04 \times 10^6$ m/s. In bulk unhybridized graphene, v_F is a sensitive probe of the strength of electron-electron interactions [2, 29], which can be screened by a large dielectric constant ϵ environment. While $v_F = 2.5 \times 10^6$ m/s on a low- ϵ quartz substrate [30], it decreases to about $1.1 - 1.4 \times 10^6$ m/s on SiO₂ [3, 21], with a limiting value of 0.85×10^6 m/s expected for infinite screening [30]. The present system can actually be envisaged as graphene on a dielectric substrate with divergent ϵ . The experimental value of v_F is in excellent agreement with the assumption of very effective screening, as expected in the immediate vicinity of a metallic ground plane.

With the above analysis it is seen that (i) the linear dispersion relation of graphene survives in the present system at both positive and negative energies and (ii) electron-electron interactions in the graphene sheet are strongly screened. This confirms that the present system thus behaves in many ways much more like graphene on a dielectric substrate rather than a graphene-metal hybridized electronic system, but within a fully screened environment.

One remaining open question concerns the physical origin of the observed quasi-particle scattering. In contrast with SiO₂, coulombic scattering centers in the form of charged impurities below the graphene do not contribute here, as these should be completely screened out by the metallic substrate. It is then tempting to envisage a localization-type interpretation to explain the DOS features in real space in Fig. 3 [31]. We have studied the variations of the features studied above (puddles and interference patterns) as a function of magnetic field and found no significant change of neither the E_D nor the G maps up to the maximum experimentally accessible magnetic field of 2 T (see Supp. Info.). This leads us to infer that

the observed interferences stem from long-range scattering by the doping inhomogeneities.

The present discussion demonstrates the realization of strongly screened graphene. The two main original features with respect to graphene on a dielectric substrate reside in the origin of doping inhomogeneities – set by the graphene-to-metal distance – and the strength of electron-electron interactions screening. This is of particular interest for possible quantitative comparisons of the Dirac physics in graphene to quantum electrodynamics (QED) [29]. While formally similar, one major difference between graphene and QED is set by the relative strengths of the coupling constants: $\alpha \propto (ev_F)^{-1} \approx 1$ in graphene and $\alpha \approx 1/137$ in QED. The tuning of α by strong screening in a large dielectric constant environment would allow recovering the weak-coupling regime in graphene and driving analogies with high-energy physics quantitative.

Acknowledgements

This work was supported by the ANR-2010-BLAN-1019-NMGEM and EU-NMP3-SL-2010-246073 GRENADA contracts. The authors are indebted to A. Tomadin, M. Gibertini, F. Guinea and M. Polini for their estimation of the influence of curvature effects. We further would like to thank L. Magaud, P. Mallet, J.-Y. Veuillen, V. Guisset, V. Bouchiat and P. David for help and stimulating discussions.

*clemens.winkelmann@grenoble.cnrs.fr

The authors declare no competing financial interests.

Methods

The experimental set-up is a home made scanning probe microscope operating inside a dilution refrigerator. Local tunnel conductance data were obtained using the lock-in technique ($V_{AC} = 6$ mV, $f=407$ Hz). Prior to cool-down, the sample is heated to 70°C overnight while pumping the chamber. During the cool-down, the sample is continuously heated well above all other inner parts of the cryostat in order to avoid cryosorption of residual gases on the sample.

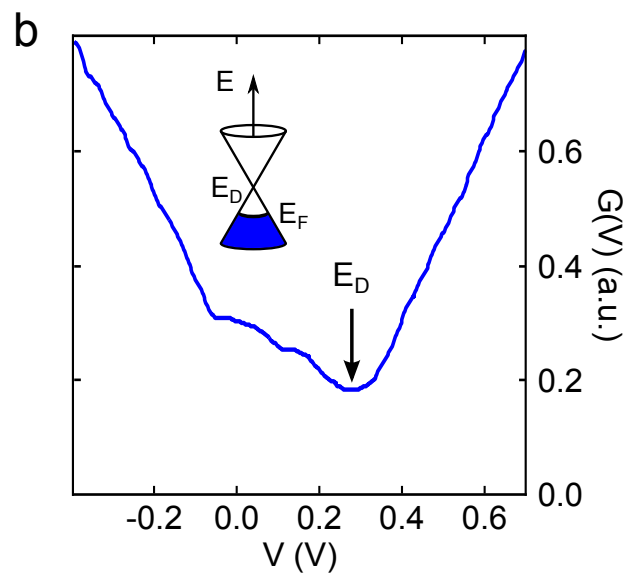
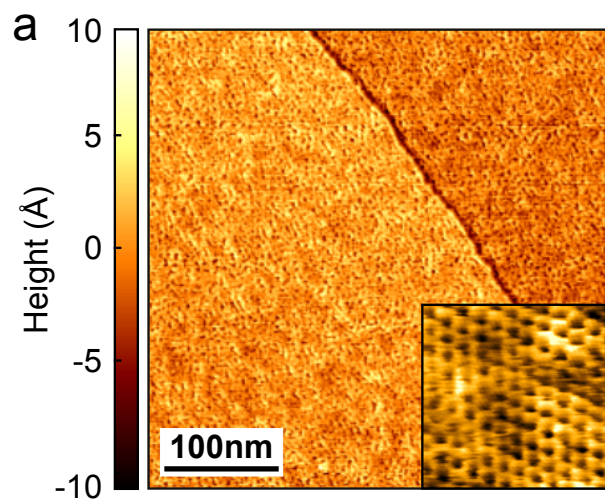
The two-dimensional mapping of $\chi(\mathbf{r})$ yields a sharp peak, at a value \mathbf{r}_0 that is usually offset from (0,0) by a few nanometers. This offset is due to drift of the residual lateral relative tip-sample position over typical DOS mapping times exceeding 50 hours. The topographic maps are therefore shifted by \mathbf{r}_0 as to maximize $\chi(0)$.

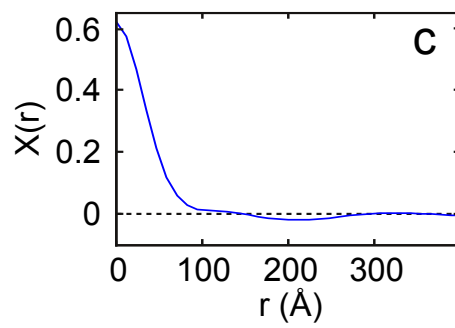
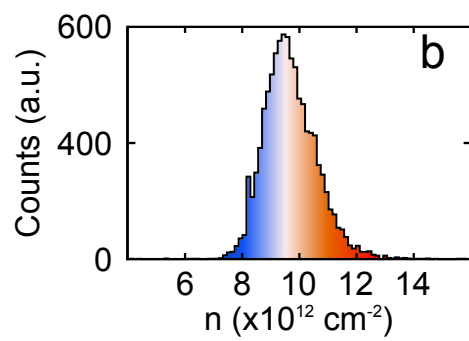
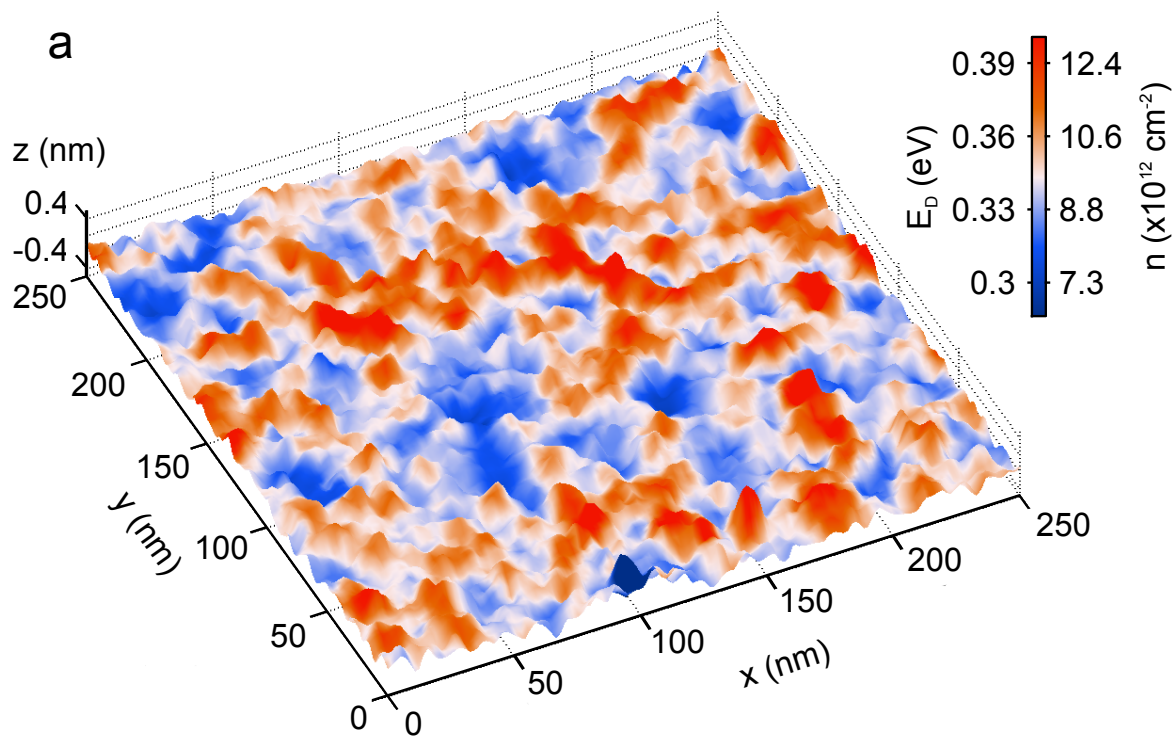
The radius $q_{max}/2$ of the interference patterns in Fig. 3 is defined as the inflection point of the angular averaged Fourier intensity (e.g. Fig. 3g), that is, the minimum of its smoothed derivative for $0.25 \text{ nm}^{-1} < k < 1 \text{ nm}^{-1}$. This criterion produces the $k(E)$ dispersion relations with least noise. This criterion however overestimates the wave vectors involved by adding a constant shift to the detected values of q , which results in the linear dispersion bands crossing at $k > 0$ in Fig. 3h.

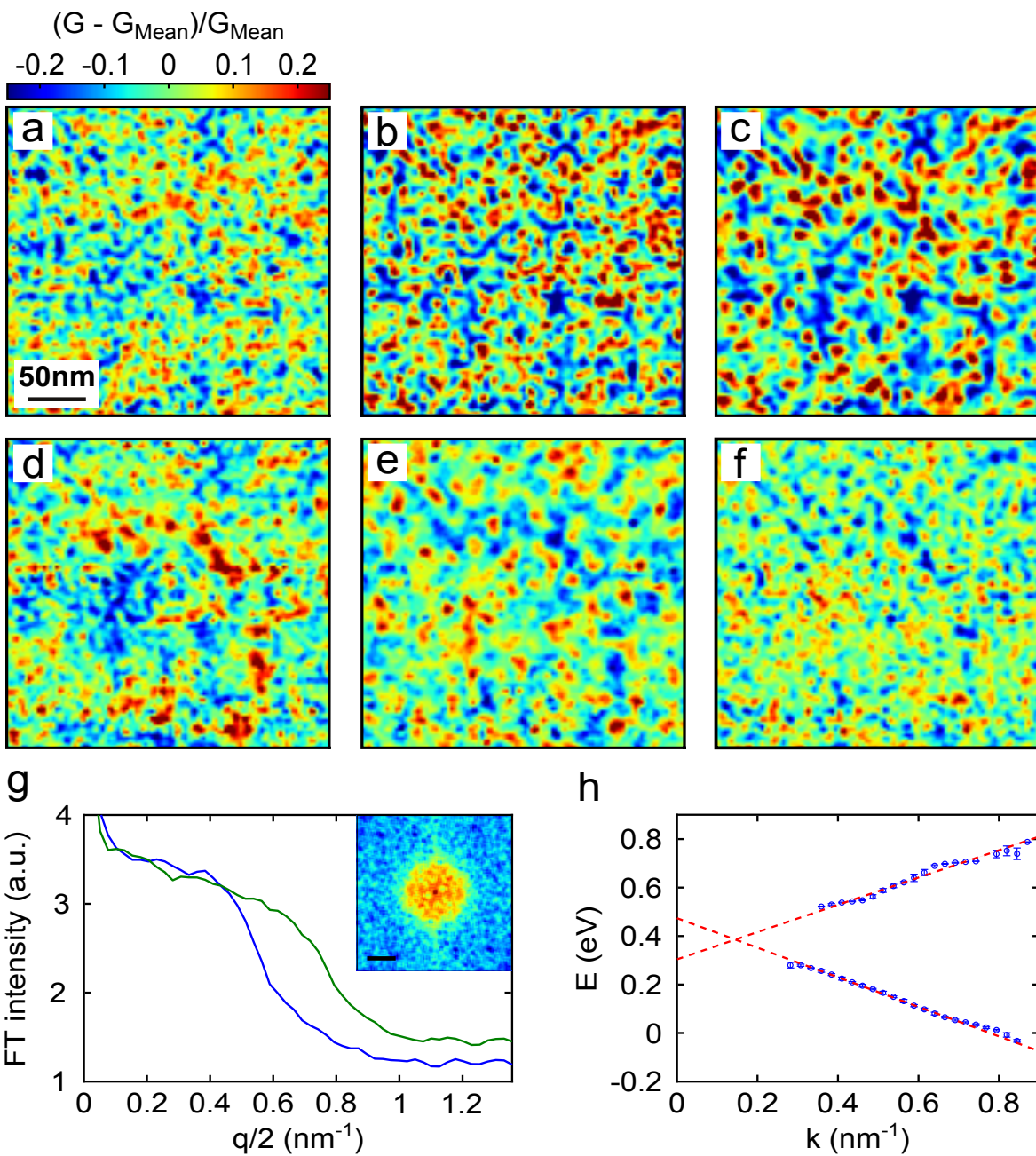
FIG. 1: Topography and density of states of graphene on iridium. (a) Scanning tunneling microscopy image on graphene on Ir(111). The image size is $400 \times 400 \text{ nm}^2$, tunnel current $I = 1 \text{ nA}$, bias voltage $V = 0.57 \text{ V}$. The atomic step in epitaxial Ir(111) covered by graphene is 2.5 \AA high. Inset: zoom-in ($2.3 \times 2.3 \text{ nm}^2$) atomic resolution image, $I = 1 \text{ nA}$, $V = 0.01 \text{ V}$. (b) Local tunneling spectroscopy $G(V) = dI/dV$ (see Methods). The Dirac point ($eV = E_D$, arrow) is defined by the minimum of G .

FIG. 2: Spatial fluctuations of the Dirac point. (a) Dirac point map (color code) superimposed with a 3D plot of the long-wavelength topography. Image of $250 \times 250 \text{ nm}^2$. (b) Carrier density distribution extracted from (a) (see text). (c) Angular average $\chi(|\mathbf{r}|)$ of the cross-correlation function (see text) between the above E_D and topography maps.

FIG. 3: Spatial inhomogeneities of the local density of states. (a) - (f) $G(\mathbf{r}, E)$ maps for $E = -185; 15; 125; 345; 555$ and 700 meV respectively. The color scale is set to cover fluctuations of $\pm 25 \%$ with respect to the average G at a given E . As the Dirac point is approached, the islands size can no longer be resolved. (g) Power spectral density from angular averaging of Fourier transform of (b) (blue) and (c) (green). The inset shows the Fourier transform of (b). The scale bar is 0.5 nm^{-1} . (h) Energy - wave vector relation extracted from Fourier analysis of the density of states maps at energy E . The dashed lines are fits to the linear dispersion relation of graphene, yielding $v_F = 0.89 \times 10^6 \text{ m/s}$ and $E_D^0 = 0.38 \text{ eV}$.







-
- [1] Martin, J., *et al.* Observation of electron-hole puddles in graphene using a scanning single-electron transistor. *Nature Phys.* **4**, 144 (2007).
- [2] Das Sarma, S., Adam, S., Hwang, E. H. & Rossi, E., Electronic transport in two-dimensional graphene. *Rev. Mod. Phys.* **83**, 407 (2011).
- [3] Zhang, Y. , Brar, V. W., Girit, C., Zettl, A. & Crommie, M. F. Origin of spatial charge inhomogeneity in graphene. *Nature Phys.* **5**, 722 (2009).
- [4] Deshpande, A., Bao, W., Miao, F., Lau, C. & LeRoy, B. Spatially resolved spectroscopy of monolayer graphene on SiO₂. *Phys. Rev. B* **79**, 205411 (2009).
- [5] Gibertini, M., Tomadin, A., Guinea, F., Katsnelson, M. I. & Polini, M. Electron-hole puddles in the absence of charged impurities. *Phys. Rev. B* **85**, 201405 (2012).
- [6] Kim, E.-A. & Castro Neto, A. H. Graphene as an electronic membrane. *Europhys. Lett.* **84**, 57007 (2008).
- [7] Partovi-Azar, P., Nafari, N. & Tabar, M. Interplay between geometrical structure and electronic properties in rippled free-standing graphene. *Phys. Rev. B* **83**, 165434 (2011).
- [8] Geringer, V., *et al.* Intrinsic and extrinsic corrugation of monolayer graphene deposited on SiO₂. *Phys. Rev. Lett.* **102**, 76102 (2009).
- [9] Ponomarenko, L. A., *et al.* Effect of a High- κ Environment on Charge Carrier Mobility in Graphene. *Phys. Rev. Lett.* **102**, 206603 (2009).
- [10] Couto, N. J. G., Sacépé, B. & Morpurgo, A. F. Transport through Graphene on SrTiO₃, *Phys. Rev. Lett.* **107**, 225501 (2011).
- [11] Das Sarma, S. & Li, Q. Graphene on SrTiO₃. *Sol. State Comm.* **152**, 1795 (2012).
- [12] Vázquez de Parga, A. L., *et al.* Periodically Rippled Graphene: Growth and Spatially Resolved Electronic Structure, *Phys. Rev. Lett.* **100**, 056807 (2008).
- [13] Wang, B., *et al.* Chemical origin of a graphene moiré overlayer on Ru(0001). *Phys. Chem. Chem. Phys.* **10**, 3530 (2008).
- [14] Sutter, P., Hybertsen, M. S., Sadowski, J. T. & Sutter, E. A. Electronic Structure of Few-Layer Epitaxial Graphene on Ru(0001). *Nano Lett.* **9**, 2654 (2009).
- [15] Pletikosić, I., *et al.* Dirac Cones and Minigaps for Graphene on Ir(111). *Phys. Rev. Lett.* **102**, 056808 (2009).

- [16] Varykhalov, A., *et al.* Ir (111) surface state with giant Rashba splitting persists under graphene in air. *Phys. Rev. Lett.* **108**, 66804 (2012).
- [17] Sutter, P., Sadowski, J. T. & Sutter, E. A. Chemistry under Cover: Tuning Metal-Graphene Interaction by Reactive Intercalation. *J. Am. Chem. Soc.* **132**, 8175 (2010).
- [18] Busse, C., *et al.* Graphene on Ir(111): Physisorption with Chemical Modulation. *Phys. Rev. Lett.* **107**, 036101 (2011).
- [19] Vo-Van, C., *et al.* Epitaxial graphene prepared by chemical vapor deposition on single crystal thin iridium films on sapphire. *Appl. Phys. Lett.* **98**, 181903 (2011).
- [20] Luican, A., Li, G. & Andrei, E. Quantized Landau level spectrum and its density dependence in graphene. *Phys. Rev. B* **83**, 041405 (2011).
- [21] Jung, S., *et al.* Evolution of microscopic localization in graphene in a magnetic field from scattering resonances to quantum dots. *Nature Phys.* **7**, 245 (2011).
- [22] Zhang, Y., *et al.* Giant phonon-induced conductance in scanning tunnelling spectroscopy of gate-tunable graphene. *Nature Phys.* **4**, 627 (2008).
- [23] Tan, Y.-W., *et al.* Measurement of Scattering Rate and Minimum Conductivity in Graphene. *Phys. Rev. Lett.* **99**, 246803 (2007).
- [24] Xue, J., *et al.* Scanning tunnelling microscopy and spectroscopy of ultra-flat graphene on hexagonal boron nitride. *Nature Mat.* **10**, 282 (2011).
- [25] Tomadin, A., Gibertini, M., Guinea, F. & Polini, M. *private communication*.
- [26] Giovannetti, G., *et al.* Doping Graphene with Metal Contacts. *Phys. Rev. Lett.*, **101**, 026803 (2008).
- [27] Rutter, G. M., *et al.* Scattering and interference in epitaxial graphene. *Science* **317**, 219 (2007).
- [28] Katsnelson, M. I., Novoselov, K. S. & Geim, A. K. Chiral tunnelling and the Klein paradox in graphene. *Nature Phys.* **2**, 620 (2006).
- [29] Castro-Neto, A. H., Guinea, F., Peres, N. M. R., Novoselov, K. S. & Geim, A. K. The electronic properties of graphene. *Rev. Mod. Phys.* **81**,109 (2009).
- [30] Hwang, C., *et al.* Fermi velocity engineering in graphene by substrate modification. *Sci. Rep.* **2**, 590 (2012).
- [31] Geim, A. K. & Novoselov, K. S. The rise of graphene. *Nature Mat.* **6**, 1832007 (2007).